2015 IEEE/RSJ International Conference on Intelligent Robots and Systems (IROS)
Congress Center Hamburg
Sept 28 - Oct 2, 2015. Hamburg, Germany

Feedback Control of a Legged Microrobot with On-Board Sensing

Remo Brühwiler, Benjamin Goldberg, Neel Doshi, Onur Ozcan,
Noah Jafferis, Michael Karpelson, and Robert J. Wood
Harvard University, John A. Paulson School of Engineering and Applied Sciences, Cambridge, MA, USA

***Abstract*— Full autonomy remains a challenge for miniature robotic platforms due to mass and size requirements of on-board power and control electronics. This paper presents a solution to these challenges with a 2.3g autonomous legged robot. An off-the-shelf optical mouse sensor is adapted for use on the Harvard Ambulatory Microrobot (HAMR) by reducing the sensor weight by 36% and achieving a position error below 11% when suspended 3mm above a cardstock surface. The position data is combined with data from a gyroscope for feedback control of both position and orientation. A microcontroller processes the sensor data and commands a controlled gait to HAMR that is powered by a battery, a boost converter and high voltage drive electronics. Solar cells are used as an alternative source providing enough power for autonomous operation of the robot. The resulting deviation for a controlled straight-line walk using both sensors to minimize lateral deviation and angular error is only 4.6%, compared to an error of 31% in an uncontrolled, straight-line walk.**

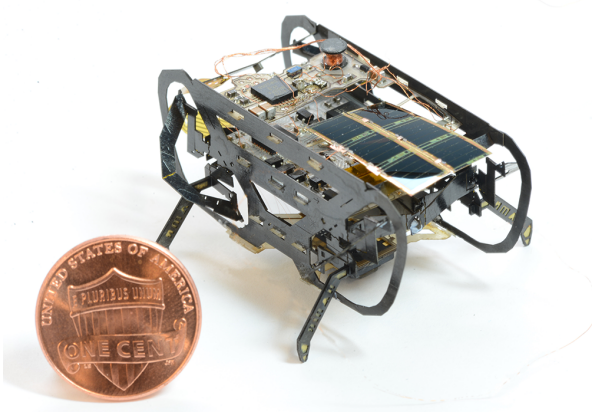

Fig. 1. HAMR-VP, modified to include on-board power, sensing and control.

I. Introduction

Small crawling robots show great potential in applications such as search and rescue, exploration of hazardous environments and infrastructure inspection. Inexpensive robots could operate in large collectives performing missions that are too dangerous for humans or require access to extremely confined spaces. Wireless and self controlled behavior is a key requirement for these applications.

Robots at larger scales such as the DASH robot [1] are able to carry on-board power and sensors but exceed 20g and are more than 10cm long. Also at a larger scale, two optical mouse sensors were used for orientation and position control of a wheeled robot [2] with feedback control implemented on-board using a microcontroller. Additionally, Fuchiwaki et al. confirmed that a combination of two optical mouse sensors (they used the Avago ADNS-2051 sensor in a piezoelectric driven microrobot) provides robust data for accurate path navigation [3]. Finally, a 10mg, solar powered, legged robot demonstrated open-loop locomotion in [4].

The legged microrobot used in this work is the Harvard Ambulatory Microrobot (HAMR). The latest version, HAMR-VP, is 4.4 cm in length, weighs 1.27 g (without on-board electronics and sensing) and has been shown to locomote at speeds exceeding to 10 body lengths per second (44 cm/s) and carry payloads greater than its own body weight while tethered to off-board power supplies [5]. Previous versions of HAMR have demonstrated on-board power and voltage amplification to drive the piezoelectric actuators ([6],[7]) but have lacked feedback control.

The desired sensor for motion control provides 2-D position and angular heading state information for real-time feedback control. An optical mouse sensor and a MEMS gyroscope are chosen as the most promising combination of sensors and is integrated into the robot. An optical mouse sensor provides position information relative to a starting point. Off-the-shelf optical mouse sensors such as the one described in this paper have the additional advantage of coming pre-packaged with signal conditioning that performs the optical flow calculations and provides velocity estimates via a standard communication protocol.

The complete system is shown in Fig.1 and a list of the mass of the components is presented in table I. Before feedback control is performed, the optical mouse sensor is characterized and the overall power requirements for the robot are determined. Locomotion properties are then investigated at low and high frequencies in section III-B. The robot is controlled with a PID controller described in section IV that varies the phase of all four lift actuators simultaneously. Varying the leg phasing allows the control system to command turns as well as performing lateral maneuvers. A minimum turning radius of 14 mm and maximum lateral speed (perpendicular to the heading of the robot) of 1 cm/s is possible.

The robot presented in this paper is the first insect-scale robot capable of on-board feedback control.

II. Sensor Characterization

The basic principle of an optical mouse sensor is the same for most packages and manufacturers. The beam coming from the sensor emitted by an LED reflects against the ground. The reflections are magnified by a lens and captured

TABLE I
MASS OF HAMR-VP WITH ON-BOARD CONTROL, SENSING AND POWER

Part	Weight
Base HAMR-VP from [5]	1270 mg
Control and Gyroscope Board	375 mg
Mouse Sensor Board	277 mg
Boost Converter Board	245 mg
Solar Cells	75 mg
Glue and miscellaneous	58 mg
Autonomous HAMR-VP	2.3 g

by an image sensor array. The sensor array passes the information to an on-board controller which calculates the deviations in x and y directions by comparing successive frames [8].

The main advantages of using an optical mouse are that the measurement is not subject to drift, they are low-cost, high precision, and have minimal computation requirements.

A. Optical Mouse Sensor for legged locomotion

Given the maximum payload carrying capacity of 1.35 g from [5], the weight limit for such a sensor must be in the range of a few hundred milligrams to be carried by the robot and allow for other power and control electronics. These tight payload constraints favor a solution with only one optical sensor. The *"low power LED integrated slim mouse sensor"* (Avago ADNS-3530) produced by Avago Technologies is chosen for position sensing due to the following benefits. The sensor is one of the smallest optical mouse sensors available on the market. In addition, it is a low power (3.6 mA active and 0.04 mA resting at 3.3 V) optical navigation sensor with an automatic power management mode, making it ideal for power-sensitive applications [9]. High speed motion is possible since the device can operate at speeds of $\sim$ 50 cm/s and accelerations of 8 g. In addition, it has an on-chip oscillator and an integrated LED to minimize external components. The chip itself is 12.9 mm in length, 9.6 mm in width and 1.69 mm in height; close to, but within the limits of HAMR's payload capacity.

Changes in position are measured by optically acquiring sequential surface images and mathematically determining the direction and magnitude of movements. The sensor contains an image acquisition system, a digital signal processor (DSP) and a four wire serial port. Surface images are processed by the DSP to determine the direction and distance of motion. This information can then be read by the microcontroller from the sensor serial port.

B. Optical Mouse Sensor Characterization

To characterize the sensor, a 3D plotter with accuracy of $\pm$ 50 µm (Shapeoko 2) is used to make specific translational movements in x-, y-, and z-directions over a white cardstock surface with the sensor attached. The intention is to read data from the sensor and compare it to the ground truth provided by the commanded plotter movements. The plotter is programmed to produce a square path at varying heights above the ground. This distance can then be compared to the sensor distance and the accuracy of the sensor as a function of distance from the ground can be determined. According to the data sheet [9] the sensor accuracy degrades with increasing distance between the sensor and the surface. Since HAMR rolls and pitches during locomotion, the sensor error at various distances is important to characterize. The sensor is moved in a square trajectory twice at each height and then the vertical distance is increased by 1 mm to measure performance at six different sensor heights.

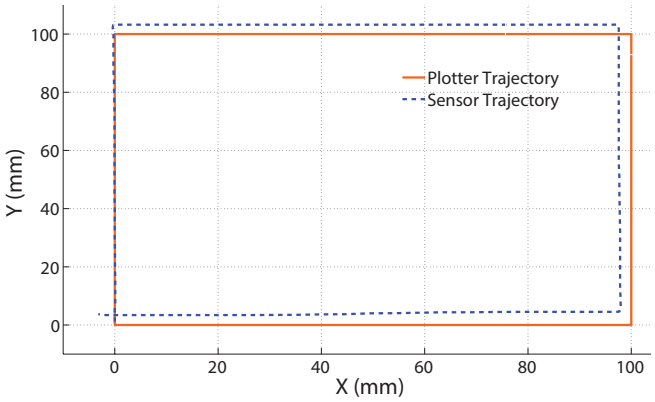

Fig. 2. A measured square trajectory is compared to a reference trajectory. The dashed blue line represents the sensor reading, and the orange line represents the reference.

An example measurement and reference trajectory are compared in Fig. 2. The error is determined by the percentage deviation of the upper right corner of the square. This is determined by computing the vector sum of the deviation of this point and dividing by the total distance traveled, in this case 20 cm in x direction and 20 cm in y direction.

Tests are performed at vertical distances of 1 mm up to 6 mm. As expected, a larger distance between the lens and the surface results in increased error as shown in Fig. 3. Based on the maximum roll and pitch rotations of 0.2 radians as measured in [10], the sensor should be placed at a nominal height of 1.5 mm in order to avoid hitting the ground. The rocking will result in a maximum height of approximately 3 mm, which, based on these measurements and the sensor characterization in Fig.3, should allow the x and y positions of HAMR to be estimated with an error of less than 10%.

The same characterization tests are conducted with the modified sensor board. To minimize the influence of the optical components (such as alignment of the lens), the measurements are taken on the exact same sensor board with some passive parts (i.e. resistors and capacitors) manually removed. The results of the tests are presented in Fig. 3. The percent path deviation of the original sensor board and the modified board are nearly identical for vertical distances between 1 mm and 5 mm. A large difference in performance is visible at a distance of 6 mm. This is most likely due to small differences in the test surface which can result in large differences in the measured distance. However, for HAMR, the maximum anticipated sensor height is 3 mm, and therefore the focus is on the region of 1 mm to 5 mm. In this

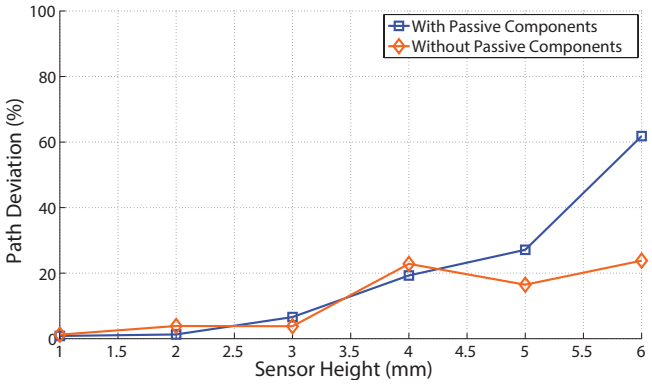

Fig. 3. The path deviation as a funciton of height with (blue) and without (orange) passive components.

target region there is no significant difference between sensor board with passive elements and without. As a result, future versions of the sensor board are built without any additional passive elements.

C. Gyroscope on HAMR

A MEMS gyroscope (Invensense, MPU9150) is used in addition to the optical mouse sensor to provide angular heading measurements. This sensor has been used and characterized on a flapping wing micro air vehicle in prior work [11] but was limited to tethered operation. The implementation of the sensor in this paper is an on-board configuration that communicates with a microcontroller (ATMEGA168).

The gyroscope utilized is a part of a 9-axis inertial measurement unit (IMU) which consists of a gyroscope, accelerometer, and magnetometer sensors on x, y, and z-axes. However, due to noise issues, the use of sensor information other than gyroscope data is avoided for this version. The sensor sends the raw gyroscope data to the microprocessor using I^2C bus, which is then filtered and integrated. The filter used is a simple, Savitzky-Golay type low pass filter. The filtered data is numerically integrated in order to find the roll-pitch-yaw angles, and the orientation of the robot is the yaw angle found with this integration.

The orientation measurements are not as accurate as presented in [11]. The main reason behind this is the simple filter that is implemented in this work. The filter in [11] is implemented on a computer running a real-time Matlab xPC operating system with built-in filter libraries; hence, there were few issues with the processing power. On HAMR, similar implementation is conducted on a microcontroller without any built-in library and very limited processing power. Using a better filter on the microcontroller would improve the orientation estimation.

III. On-Board Position Sensing

The optical mouse sensor board consists of a lens, the optical mouse sensor and a supporting PCB. The integration of these three components is discussed in this section with special attention paid to the weight-saving modifications.

A. Making the Sensor Lighter

To reduce unnecessary weight, sections of the base plate can be removed by laser micro-machining excess material off the PCB typically intended for mounting the sensor. Small sections of the PCB that contain vias and support the semiconductor elements will remain. The original sensor weight is reduced from 244 mg to 204 mg.

The "lens plate" consists of two crucial elements: The first is a plastic molded illumination lens and the second is an imaging lens used for magnification. Those two elements are located close to each other, covering the LED and the photo array of the sensor. With a simple rectangle shaped cut profile everything but those two elements can be removed and the original lens weight of 125 mg can be reduced to 32 mg. Fig.4 shows the lens and sensor after these weight reduction steps.

A crucial part of making a light sensor board is designing a lightweight and sturdy PCB. The PCB supports the sensor and holds it in place under the robot providing reliable electrical and mechanical contact.

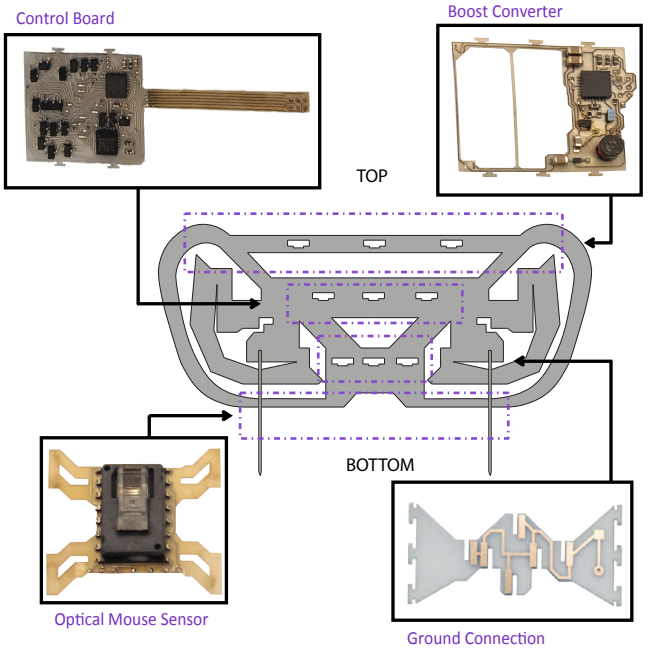

Fig. 4. The optical mouse sensor including lens stack (bottom left). The board is connected mechanically on all four sides of the "X" shape to the bottom of the robot and electrically with manually soldered wires to the control board. The control board (top left) includes the microcontroller, gyroscope, programming 'tail', and electrical and mechanical connections to the actuators. The boost converter board (top right) amplifies a low voltage supply (e.g. from a battery or solar cells) to the 200V operating point for the piezoelectric actuators. Electrical and mechanical ground connections to the actuators (bottom right). All boards are connected electrically by manually soldering individual strands of wire to the control board.

Fig. 4 presents the integration with the sensor board ready for HAMR. After fabrication of the 37mg PCB, the optical mouse sensor is soldered to the PCB using a reflow process. In a last step the protective covering on the lens is removed and the lens (after cutting away the unnecessary parts) is glued on top of the sensor above the LED and the photo

array. This has to be done carefully as accurate alignment of the lens to the photo array is crucial for good sensor readings. The complete sensor board weighs 277mg and is shown in Fig. 4.

B. Results with on-board sensing

The sensor board is then mounted to the bottom of HAMR by attaching the four arms of the 'X' shaped PCB to the two bottom composite rails of the robot with cyanacrolate glue.

For initial tests, the sensor is wired to an off-board Arduino for computation and communication. The test setup in this case consists of two independent systems: One is the "robot" setup which includes HAMR, a computer controlling the robot, and a power source. The second system is the "sensor" system which consists of the sensor board, an Arduino, and a laptop to collect the data coming from the Arduino. Those two systems are connected electrically via a tether to HAMR. The force imparted from the tether has a negligible effect on the walking motion.

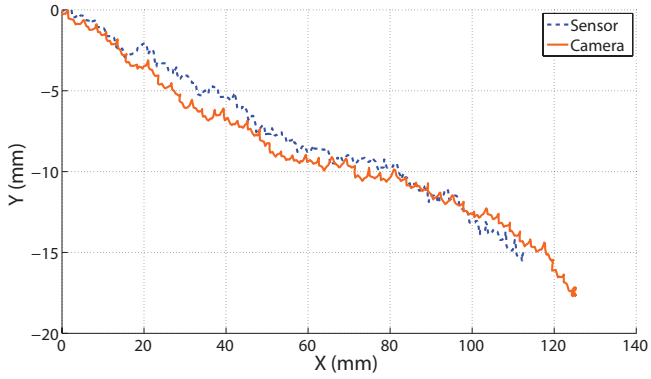

Fig. 5. A test walk of HAMR at 10Hz walking frequency with the attached sensor. Both lines represent the trajectory traveled by HAMR in body coordinates.

The results from a walking test at 10Hz is shown in Fig. 5. Data from the sensor is plotted against data from an overhead camera and vision tracking (Phantom v7.3 and Xcitex-Pro Analyst) with an accuracy of ± 0.5mm. The tracking software determines the center of mass and orientation of the robot which are transformed into the body coordinates and are plotted in Fig. 5. The error in Fig. 5 can be calculated by comparing error in the total distance in X and Y directions between the sensor and the camera. For a trial with the robot running at a frequency of 10Hz, the cumulative, straight-line error is 10.22%. These results are consistent with the initial accuracy estimations from the 3D plotter tests in section II-B for a sensor height between 3-4mm.

To determine if the walking frequency influences error, further tests are conducted. For example, the gait frequency could influence rocking which would result in significant up and down movement of the lens relative to the surface. As investigated in the previous sections, this difference in height affects the accuracy of the system. To understand how the speed influences the error, two additional measurements are conducted at 20Hz and 30Hz. For the 20Hz test, an error of approximately 8.28% was observed whereas the resulting error of the 30Hz test was approximately 11.18%.

The first conclusion is that the sensor measurement is consistently less than the camera measurement for all tested frequencies. This indicates that the sensor "loses" data on the way. This might be because of the vertical movement of the robot; HAMR could be lifted out of the range of the sensor for a short time during the step (too far away from ground) and could lose the distance traveled during this time. This error is exacerbated by other sources of error including lens contamination and surface imperfections.

The second and most important conclusion is that the sensor error is in the range of 8% to 11% which is sufficient for use in HAMR position control. The error seems not to be influenced by the traveling speed of the robot. Furthermore, the sensor has to be mounted as close as possible to the ground and while taking the walking motion of HAMR into account (up and down movement of the sensor) a maximum error between 8% to 11% is to be expected.

IV. Feedback Control on HAMR

This section describes the integration of the optical mouse sensor, a gyroscope, a microcontroller and power electronics to control the actuators. The only connection to the robot is a four wire tether which provides power (200V as well as 3.3V), a ground connection and a debugging wire. In Fig. 1, HAMR is shown with a top PCB that includes a controller (ATmega168), power electronics and a gyroscope (MPU-9150). The bottom PCB carries the optical mouse sensor.

A. Closed Loop Control of HAMR

Two manually tuned PID controllers (see Fig. 6) minimize the error between the measured orientation and position and the desired values.

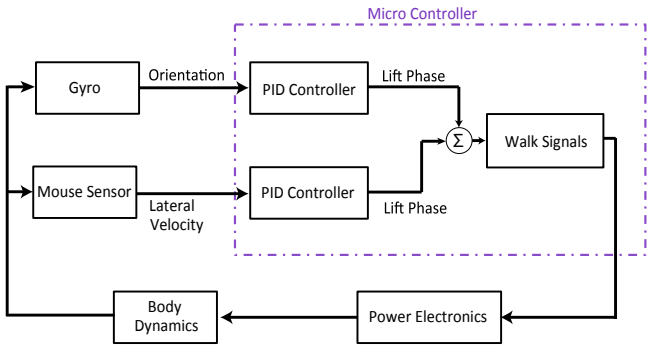

Fig. 6. Schematic of the on-board control loop. Both sensors provide data which are fed into the microcontroller (right) resulting in drive signals to the actuators.

The feedback controller takes the measured angle and lateral deviation as well as both desired values into account and calculates the resulting orientation phase and 'crabbing' (lateral) phase. The orientation phase and crab phases are added to the nominal gait phasing. These updated values are then read by the signal generation block to achieve the desired path. The actuator drive scheme and leg phasing

TABLE II

LEG PHASING FOR ORIENTATION AND LATERAL CONTROL

Leg	Nominal Lift Phase w.r.t Swing	Orientation o_c	Lateral Position l_c
Front Left	90°	$+\phi_1$	$+\phi_2$
Front Right	90°	$-\phi_1$	$-\phi_2$
Rear Right	90°	$-\phi_1$	$+\phi_2$
Rear Left	90°	$+\phi_1$	$-\phi_2$

for turning is explained in detail in [5]. The commanded signal phase for each leg is controlled independently and is calculated as the following: $\phi = 90° + o_c + l_c$ with o_c and l_c defined in table II. The two independent PID controllers update ϕ_1 and ϕ_2 of table II as defined in equations (1) and (2).

$$\phi_1 = K_p^{or} e^{or} + K_d^{or} \frac{d}{dt} e^{or} + K_i^{or} \int e^{or} \tag{1}$$

$$\phi_2 = K_p^{lat} e^{lat} + K_d^{lat} \frac{d}{dt} e^{lat} + K_i^{lat} \int e^{lat} \tag{2}$$

where $K_p^{\{or,lat\}}, K_d^{\{or,lat\}}, K_i^{\{or,lat\}}$ are PID gains for the orientation and lateral controllers and e^{or} and e^{lat} are orientation and lateral errors, respectively.

The control loop executes functions including walking and updating variables such as sensor values and control commands. The only function which is executed in every iteration is the signal generation, (block "Walk Signals" in Fig. 6) which runs at 1kHz and takes the most recent output of the PID controller as an input and defines the required leg phases based on table II to achieve the desired trajectory.

The sensor readings must be limited below their maximum bandwidth to achieve a walking frequency of 10 Hz given the choice of microcontroller. For example, the position measurement from the optical mouse sensor is updated at 100 Hz, the gyroscope is updated at 25 Hz, and the control values (corrections to the nominal gait phasing) are updated at $\sim$ 3 Hz. The presented update rates are experimentally found to be the minimum update rates required for accurate trajectory following at 10 Hz leg actuation. One main consideration is that the gyroscope takes significantly longer to update compared to the the control commands or the optical mouse sensor values since the signal must be filtered and integrated to obtain the robot heading. However, if the update doesn't take place regularly, the angular error increases drastically.

B. Straight trajectories

Performing a straight walk is possible when feedback control with both sensors is used. The lateral deviation as well as the angle of the robot relative to the desired trajectory are minimized. With an overhead camera, a high speed video of HAMR is taken while performing a straight line walk (Phantom v7.3). A second trial for an uncontrolled walk is performed to compare both deviations from the desired trajectory. The two videos are then processed with a video tracking software (Xcitex-Pro Analyst) to extract the trajectory of the center of mass.

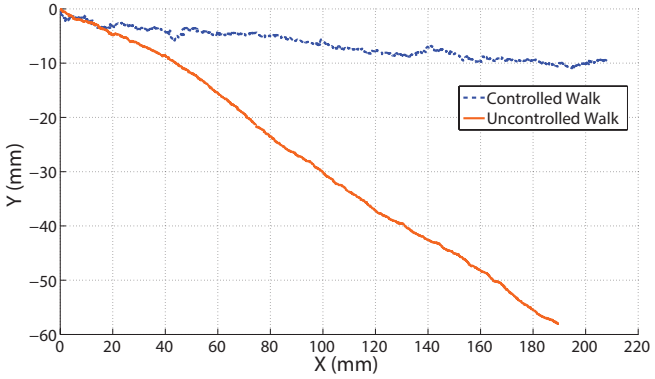

Fig. 7. Results of tracking the center of mass of the robot. The line in blue shows the path of HAMR performing a controlled walk and the orange line allows a comparison with an uncontrolled walk.

Fig. 7 shows the tracked center of mass for controlled and uncontrolled motions starting at the origin with an angle of zero degrees between the robot and the x-axis. HAMR performs a straight walk for 200mm. This results in an error of 4.6% lateral deviation for the controlled case in comparison to 31% path error for an uncontrolled walk.

The explanation for the error in an uncontrolled walk likely lies in asymmetric mechanics. For example, if one transmission swings or lifts slightly more than the others, this can result in small but constant crabbing and turning motions. These accumulating errors can be verified by investigating the lateral deviation and heading angle presented in Fig. 7.

Errors arising from walk mechanics can be minimized with the two sensors and the presented feedback controller. The reason for the closed-loop error of 4.6% is likely due to imperfections in the sensors. In the controlled walk, both the lateral and orientation errors are zero at the end of the walk when observed through the debugging line. This indicates that an error in the angle as well as in the lateral deviation has developed without being measured by the sensors. Most likely this is due to noise, slow update rates, drift in the IMU, and the fact that both "lose measurements" as described in section II-B where the error increases if the sensor is not close enough to the ground.

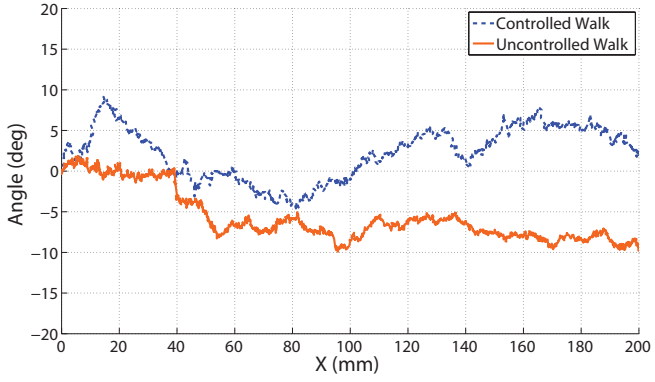

Fig. 8. The angle of the robot for the uncontrolled walk (orange) and controlled case (blue).

A robust minimization of the heading deviation is difficult due to the characteristics of the gyroscope. First, a filter has to be applied to extract reliable data from the noisy readings. Second, an integration of the angular velocity in the main loop can result in poor estimation because a) the update rate might not be fast enough (ideally the gyroscope should be read at 1kHz or higher), b) the shaking and rocking motions of HAMR might affect readings and c) the gyroscope's inherent drift in time. Therefore it is challenging to extract one resulting angle in the z direction only. Nevertheless the estimated angle of the gyroscope was used in the feedback loop and roughly minimized (see Fig. 8). This resulted in an oscillation around the x axis which is closer to a straight walk than a constantly increasing angular error when uncontrolled. The RMS error of the heading in the trial shown in figure 8 for the controlled walk is 3.6% compared to 6.3% in the the uncontrolled walk.

V. On-Board Power

On-board power is a crucial element of autonomy. First, the power consumption must be analyzed in order to evaluate possible supply or storage mechanisms. Those sources must match the requirements of HAMR, including a weight limit of approximately 1.35g for all additional systems including sensing and control.

Two sources, a battery ("GM300910" from PowerStream) and solar cells ("ELO solar cells 1-6615-8" from MicoLink Devices) are successfully tested for this HAMR version. The same boost converter works in both cases.

A. Power Consumption

The power consumption is a critical factor for an on-board power supply as the source, which has to meet the demand and at the same time not degrade walking significantly. An investigation is conducted to determine the power requirements of the robot by measuring the voltage and the current for the 3V line and the 200V line separately. With those measurements, a total power consumption is determined.

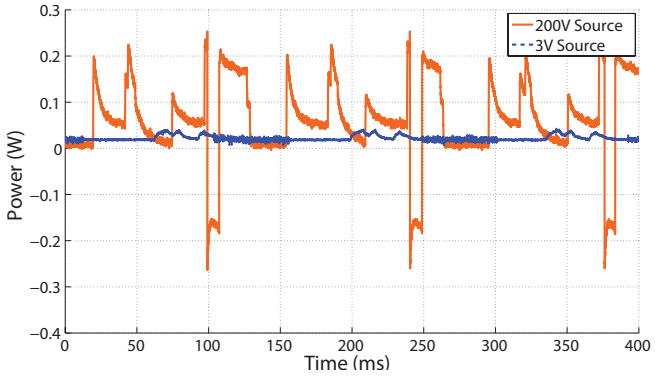

Fig. 9. Power of HAMR when walking. The orange line is the power consumption of the high voltage line (primarily due to actuators and power electronics) and the blue is the 3V supply (mainly controller and sensors).

Fig. 9 shows the resulting plot of both power measurements. As expected, both plots reveal a certain periodicity for a gait frequency of around 6 to 7Hz. Averaging over the power consumption of the low voltage line results in 22.0mW. Doing the same for the high voltage part reveals that a supply has to meet 60.1mW to power the 200V line for a total of 82.1mW average power consumption. Considering the fact that higher peak power is needed (as can be seen in Fig. 9) and the efficiency of the boost converter (72% at maximum according to [12]) has to be taken into account, this 82.1mW is a rough approximation of the minimal power requirements.

B. Power Source

Two power sources are considered for this prototype: A battery and solar cells. Batteries have already been successfully used for previous HAMR versions in [7], however batteries have the drawback of low energy density resulting in short lifetime and/or large relative mass. The tests in [7] successfully demonstrated walking at an actuation frequency of 20Hz for two minutes using a 330mg, 8mAh lithium polymer battery ("GM300910" from PowerStream).

Recent advances in solar cell fabrication has increased the efficiency (up to 30%) for very thin-film cells. The solar cells in a 2S3P configuration can provide up to 240mW with a very bright flashlight ("The Torch" from Wicked Lasers) 6 inches above the cells, or approximately four Sun's of luminosity. Tests have shown that currents of around 47mA at a voltage of 5V are achieved in these conditions. These specifications fit well with the power requirements and payload capacity of HAMR with an overall weight of 75mg and an area of 19mm in length and 12mm in width.

C. Boost Converter

A tapped-inductor boost converter is used for DC-DC conversion, which is a combination of conventional boost and flyback converters and is outlined in [12]. This technique offers several advantages, especially for low power and high voltage applications. Also it can be miniaturized while maintaining reasonable efficiency which is important for small scale robots.

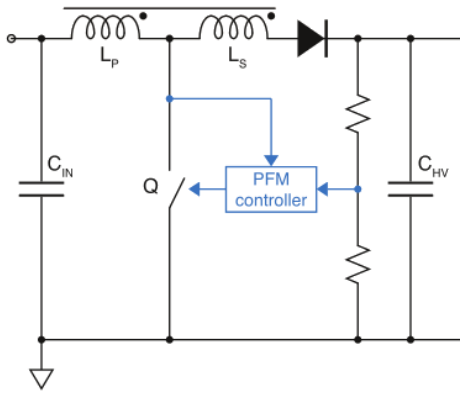

Fig. 10. Schematic of the boost converter. It consists of an input and output capacitor as well as a tapped inductor in the upper left corner. The feedback path is completed with a resistor divider which is read by the controller. The output of the controller, Q, is a frequency controlled semiconductor switch (modified from [12]).

During a typical switching cycle, the switch Q (see Fig. 10) is turned on, and current builds up in the primary winding (marking L_P). As Q is turned off, the energy stored in the magnetic core is discharged to the high voltage output through both windings. In this manner the capacitor, C_{HV}, is charged. To control the output voltage a controller is needed which modulates the switching frequency. This is represented by the blue "PFM controller" block in Fig. 10. The output is monitored using a resistor divider and an analog comparator. If the voltage falls beneath a certain level a switching cycle is initiated delivering energy to the output capacitor and the load.

D. On-Board Power Results

With the 8mAh battery a HAMR can walk for approximately 3 minutes. During this time all sensors were on and reading continuously. Furthermore both microcontrollers (one on the control board and one in the power converter) were running. Having a separate microcontroller for the boost conversion allows the sensor and leg controller to maintain the same gait frequency and sensor accuracy.

An alternative to the use of batteries is depicted in Fig. 1. The solar cells were demonstrated to provide sufficient power to autonomously actuate HAMR's legs. Feedback control tests, however, were unable to be performed due to the heat of the light source which warped the cells and electrical connections and did not allow enough time for the experiments to be conducted. As the cells are significantly lighter than the batteries, though, it is feasible to carry more than six cells and operate in reduced intensity light; eventually this can allow HAMR to perform a controlled walk, even on a cloudy day.

VI. Conclusion

A 2.3g autonomous device with control and sensing abilities is presented. Sensing both angle and position of the robot provides the ability for path control; for example, a straight line walk is successfully demonstrated. The sensor data is sufficient for this application, although faster and better filtered readings from the gyroscope can improve the heading control accuracy. A detailed investigation of position data offered by the optical mouse sensor showed good accuracy and robustness to HAMR's walking dynamics. The on-board control of the robot successfully minimized the errors in angle and lateral deviation with the provided sensor data. On-board power can be provided by either a battery or solar cells feeding a DC-DC converter. With all of these systems on-board, HAMR is able to sense and control the path autonomously. Future work will investigate new control strategies for arbitrary trajectory following, wireless communication and additional sensing capabilities. Furthermore, custom integrated circuits (similar to those in [13]) will be investigated to achieve lower component weights and faster sensing and actuation frequencies.

VII. Acknowledgments

The authors would like to thank all Harvard Microrobotics Laboratory group members for their invaluable discussions. This work is partially funded by the Wyss Institute for Biologically Inspired Engineering and the National Science Foundation. This material is based upon work supported by the National Science Foundation Graduate Research Fellowship under Grant Number DGE1144152. Any opinion, findings, and conclusions or recommendations expressed in this material are those of the authors and do not necessarily reflect the views of the National Science Foundation.

References

[1] P. Birkmeyer, K. Peterson, and R. S. Fearing, "Dash: A dynamic 16g hexapedal robot." IEEE, 2009, pp. 2683–2689.

[2] J. Cooney, W. Xu, and G. Bright, ""Visual dead-reckoning for motion control of a Mecanum-wheeled mobile robot"," *MECHATRONICS*, vol. 14, no. 6, pp. 623–637, JUL 2004.

[3] O. Fuchiwaki, N. Tobe, H. Aoyama, D. Misaki, and T. Usuda, "Automatic micro-indentation and inspection system by piezo driven micro robot with multiple inner sensors," in *2005 IEEE International Conference on Mechatronics and Automations, Vols 1-4, Conference Proceedings*, Gu, J and Liu, PX, Ed. IEEE, 2005.

[4] S. Hollar, A. Flynn, C. Bellew, and K. Pister, "Solar powered 10 mg silicon robot," in *Micro Electro Mechanical Systems, 2003. MEMS-03 Kyoto. IEEE The Sixteenth Annual International Conference on*. IEEE, 2003, pp. 706–711.

[5] A. T. Baisch, O. Ozcan, B. Goldberg, D. Ithier, and R. J. Wood, "High speed locomotion for a quadrupedal microrobot," *The International Journal of Robotics Research*, p. 0278364914521473, 2014.

[6] M. Karpelson, B. H. Waters, B. Goldberg, B. Mahoney, O. Ozcan, A. Baisch, P.-M. Meyitang, J. R. Smith, and R. J. Wood, "A wirelessly powered, biologically inspired ambulatory microrobot," in *Robotics and Automation (ICRA), 2014 IEEE International Conference on*. IEEE, 2014, pp. 2384–2391.

[7] A. T. Baisch, C. Heimlich, M. Karpelson, and R. J. Wood, "HAMR3: An Autonomous 1.7g Ambulatory Robot," in *Intelligent Robots and Systems (IROS), 2011 IEEE/RSJ International Conference on*. IEEE, 2011, pp. 5073–5079.

[8] D. Sekimori and F. Miyazaki, ""Precise Dead-Reckoning for Mobile Robots using Multiple Optical Mouse Sensors"," *Springer Netherlands*, vol. 76, no. 2, pp. 145–151, 2007.

[9] Avago Technologies Inc., "ADNS-3530 Optical Mouse Sensor Data Sheet," *www.avago.com*, 2014.

[10] B. F. Seitz, B. Goldberg, N. Doshi, O. Ozcan, D. L. Christensen, E. W. Hawkes, M. R. Cutkosky, and R. J. Wood, "Bio-inspired mechanisms for inclined locomotion in a legged insect-scale robot," in *2014 IEEE International Conference on Robotics and Biomimetics (ROBIO) , December 5-10, 2014, Bali, Indonesia*, 2014, pp. 791–796.

[11] S. Fuller, A. Sands, A. Haggerty, M. Karpelson, and R. Wood, "Estimating attitude and wind velocity using biomimetic sensors on a microrobotic bee," in *2013 IEEE International Conference on Robotics and Automation (ICRA)*, 2013 2013, Conference Paper, pp. 1374–80, 2013 IEEE International Conference on Robotics and Automation (ICRA), 6-10 May 2013, Karlsruhe, Germany.

[12] M. Karpelson, G.-Y. Wei, and R. J. Wood, "Driving high voltage piezoelectric actuators in microrobotic applications," *SENSORS AND ACTUATORS A-PHYSICAL*, vol. 176, pp. 78–89, APR 2012.

[13] X. Zhang, M. Lok, T. Tong, S. Chaput, S. K. Lee, B. Reagen, H. Lee, D. Brooks, and G.-Y. Wei, "A multi-chip system optimized for insect-scale flapping-wing robots."